Limits of the Hydrodynamic No-Slip Boundary Condition

Yingxi Zhu and Steve Granick

Department of Materials Science and Engineering, University of Illinois, Urbana, Illinois 61801

(Received 29 October 2001; published 26 February 2002)

A controversial point in fluid dynamics is to distinguish the relative importance of surface roughness and fluid-surface intermolecular interactions in determining the boundary condition. Here hydrodynamic forces were compared for flow of Newtonian fluids past surfaces of variable roughness but similar, poorly wetted, surface chemistry. The critical shear stress and shear rate to observe deviations from predictions using the no-slip boundary condition increased nearly exponentially with increasing roughness and diverged at ≈6 nm rms roughness. We conclude that local intermolecular interactions dominated when the surface was very smooth, but roughness dominated otherwise. This quantifies the limits of both ideas.

DOI: 10.1103/PhysRevLett.88.106102 PACS numbers: 68.08.–p, 68.35.Md

For many years it has been observed that there is no compelling argument to justify the standard "no-slip" boundary condition of textbook continuum hydrodynamics, which states that fluid at a solid surface has no relative velocity to it [1]. However, this assumption successfully describes much everyday experience. Indeed, Feynman [1] noted in his Lectures that the no-slip condition explains why large particles are easy to remove by blowing past a surface, but small particles are not. Similarly, readers who wash dishes have noticed that it is difficult to remove all the soap just by running water—a dishcloth is needed for effective cleaning. Why?

There are two schools of microscopic explanation. The traditional explanation is that since most surfaces are rough, the viscous dissipation as fluid flows past surface irregularities brings it to rest, regardless of how weakly or strongly molecules are attracted to the surface [2–4]. This has been challenged by accumulating evidence that, if molecularly smooth surfaces are wet only partially, hydrodynamic models work better when one uses instead "partial slip" boundary conditions [5–14]. Then the main issue is whether fluid molecules attract the surface or the fluid more strongly [5–12,15]. In this study we tested the limits of both ideas. To the best of our knowledge, this is the first experimental study in which roughness was varied systematically at the nanometer level.

To study this slippery question, the starting point was a modified surface forces apparatus whose step-free single crystals of muscovite mica were coated with methyl-terminated self-assembled organic monolayers. Briefly, surface spacing was measured using optical interferometry and dynamic forces were measured using piezoelectric methods [12]. We analyzed the viscous response, 90° out of phase with the sinusoidal drive. The separation D was measured relative to $D = 0$ in adhesive contact in air.

Figure 1 sketches the experimental strategy and shows AFM (atomic force microscopy) images of some of the surfaces that we studied. Three strategies were used to vary roughness systematically. The first was based on using collapsed polymers. Narrow-distribution diblock copolymers of polystyrene ($M_w = 55\,400$) and polyvinylpyridine ($M_w = 28\,200$), PS/PVP, were allowed to adsorb for a limited time from a dilute (5×10^3 μg mL^{-1}) toluene solution. The remaining bare regions of mica were then coated with an organic monolayer of condensed octadecyltriethoxysilane (OTE) [13]. The contact angles against water and tetradecane were stable in time, which shows that the liquids did not penetrate them. AFM images in Fig. 1 quantify the roughness (and show that aggregation occurred during some step of the preparation procedure). To produce larger roughness, mica was coated with condensed octadecyltrichlorosilane (OTS) after first saturating the cyclohexane deposition solution with H_2O to encourage partial polymerization in solution before surface deposition. In the third method, self-assembled monolayers of alkane thiols were formed on silver whose roughness was controlled by the dc bias applied during sputter deposition. The silver was coated with octadecanethiol (Aldrich) deposited from ethanol solution (0.5 mM) and placed in opposition with a molecularly smooth OTE surface. Surface separation was then measured between silver films on the back sides of the mica sheets (methods 1 and 2) or between silver on the front side of one sheet and the back side

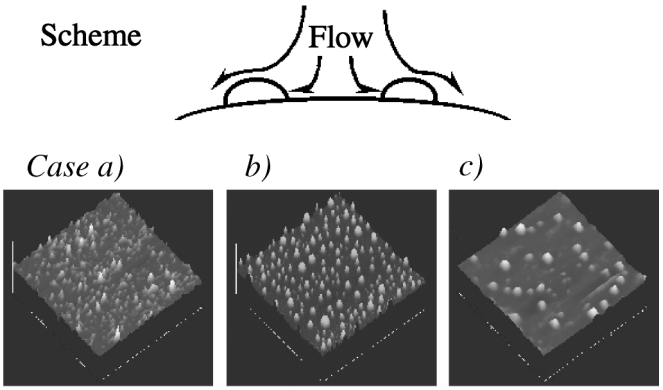

FIG. 1. The scheme of flow over a rough surface is shown schematically in the top portion of this figure. In the bottom panels, AFM images are shown of the following cases: (a) self-assembled OTS layers; (b) PS/PVP-OTE layers (surface coverage ~80%); (c) PS/PVP-OTE layers (surface coverage ~20%). Each AFM image concerns an area 3 μm × 3 μm.

TABLE I. Contact angles and surface roughness (θ_a, advancing; θ_r, receding). Case *a*: self-assembled OTS layers; case *b*: PS/PVP-OTE layers (surface coverage ~80%); case *c*: PS/PVP-OTE layers (surface coverage ~20%); case *d*: smooth OTE monolayers; case *e*: self-assembled octadecanethiol monolayer on silver; case *f*: self-assembled octadecanethiol monolayer on silver. The rms roughness was measured over areas 3 μm × 3 μm. The AFM characterization was performed in contact mode in air using a Nanoscope III and a Si_3N_4 top (Digital Instruments). The contact angles have an uncertainty of ±2°.

Sample		Case *a*	Case *b*	Case *c*	Case *d*	Case *e*	Case *f*
Water	θ_a	105°	110°	110°	110°	121°	121°
	θ_r	75°	85°	90°	110°	112°	98°
Tetradecane	θ_a	35°	38°		38°	42°	42°
	θ_r	12°	21°		38°	32°	25°
rms roughness		6 nm	3.5 nm	2 nm	0.2 nm	0.5 nm	1.2 nm

of the adjoining sheet (method 3). Table I shows that the advancing contact angle was similar in all cases but that the receding contact angles depended on surface roughness, which was evaluated using atomic force microscopy.

The principle of hydrodynamic measurement was simple. Two solids of mean radius of curvature R (≈2 cm in the experiments reported below), at spacing D, experience hydrodynamic forces F_H as they approach one another (or retreat from one another), thereby squeezing fluid out of (or into) the intervening gap. This force is proportional to the rate at which spacing changes, dD/dt (t denotes time), and inversely proportional to D. The no-slip boundary condition combined with the Navier-Stokes equations gives to first order the following expression, known as the Reynolds equation:

$$F_H = f^* \frac{6\pi R^2 \eta}{D} \frac{dD}{dt}, \qquad (1)$$

and high-order solutions essentially confirm this, the lowest-order term. We introduce f^*, the dimensionless number that quantifies, if $f^* \neq 1$, deviation from the classical prediction. The prediction is analogous when the surface spacing is vibrated [14]. A sinusoidal drive produces an oscillatory hydrodynamic force whose peak we denote as $F_{H,\mathrm{peak}}$. The peak velocity is $v_{\mathrm{peak}} = d\omega$, where d is the vibration amplitude and ω is the radian frequency of vibration. The amplitude and frequency were controlled independently, allowing the mean velocity to vary over a wide range without a large change of the film thickness. It is known that data obey Eq. (1) when the fluid wets the solids [14,16,17]. Control experiments using a spectrum analyzer revealed no harmonics in the hydrodynamic responses indicating that flow produced a steady state whose lifetime exceeded the period of oscillation (see further discussion below).

Figure 2 illustrates raw data. The top panel concerns deionized water, the bottom panel tetradecane. The main figure plots hydrodynamic force against surface separation for experiments at a given velocity. The inset in each panel shows a quantity proportional to the inverse hydrodynamic force, the damping function (defined in the figure legend), plotted against surface separation. The no-stick boundary condition predicts linear dependence in this representation. Taken together, these data show that the rougher the solids, the better the agreement with the no-slip assumption.

What are possible complications? The confinement-induced enhancement of fluid viscosity and ensuing shear thinning have seen much discussion [18], but those effects

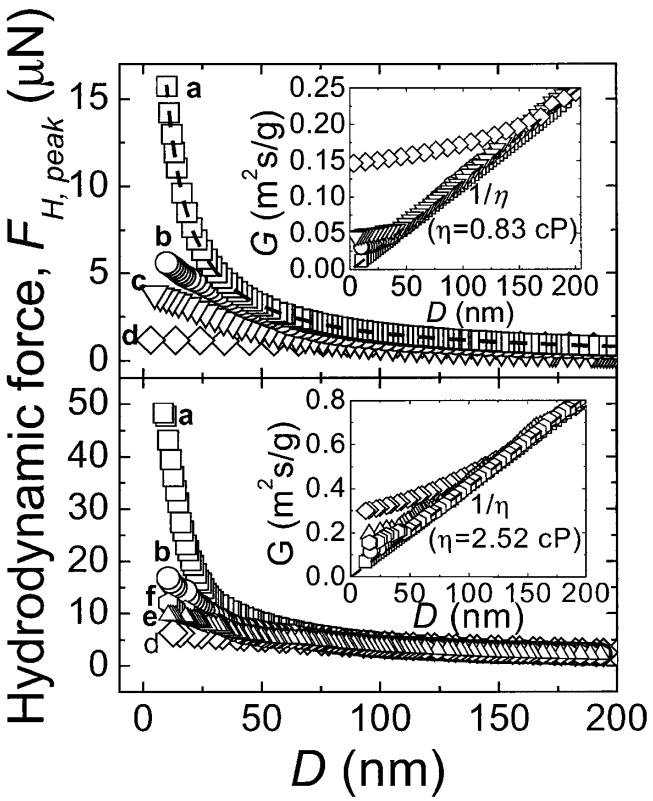

FIG. 2. Hydrodynamic force between crossed cylinders, $F_{H,\mathrm{peak}}$, is plotted against surface separation D for tetradecane (bottom panel) and deionized water (top panel) undergoing 1 nm vibrations at 63 rad s^{-1} ($v_{\mathrm{peak}} = 63$ nm s^{-1}). The rms roughness was 6 nm (case *a*; squares), 3.5 nm (case *b*; circles), 2 nm (case *c*; down triangles), 1.2 nm (case *f*; hexagons), 0.6 nm (case *e*, up triangles), and molecularly smooth (case *d*; diamonds). The inset in each panel shows the damping function, $G = 6\pi R^2 v_{\mathrm{peak}}/F_{H,\mathrm{peak}} = D/\eta$, plotted against D. The reciprocal of the slope in the linear portion of the inset gives the known viscosity of these fluids. Given the no-slip boundary condition and a Newtonian fluid, G should extrapolate to the origin. The observed curvature implies a breakdown of the no-slip boundary condition.

extrapolate to zero beyond a film thickness of 5–10 molecular dimensions. They should not arise for the thicker films studied here. In addition, we emphasize that the conclusions in this Letter are not chemically specific. They hold for the Newtonian polar fluid (water) and the Newtonian nonpolar fluid (tetradecane) alike.

How should these data be compared? Our recent study involving flow past partially wetted *smooth* surfaces showed, when the frequency and amplitude of oscillatory flow were varied, that the data depended on the peak velocity, their product, v_{peak} [11]. Furthermore, deviations from Eq. (1) depended on v_{peak}/D; the flow rate, which is the ratio, is suggested by the form of Eq. (1) [11]. In this new study, the same functional form was found to collapse the data also when roughness was varied. Evidence for this is shown by the comparisons at variable v_{peak} and D shown in Fig. 3, where the data are plotted as a function of v_{peak}/D on log-log scales. We emphasize that f^* is used as a fitting parameter to which we do not assign physical meaning. The "stick" prediction ($f^* = 1$) is a horizontal line and one observes that deviations from this decreased as roughness increased. A possible mechanism for rate dependence was proposed by de Gennes [19]. He conceives that shear induces the nucleation of vapor bubbles; once the nucleation barrier is exceeded they grow to cover the surface, and flow of liquid is over this thin vapor film rather than the surface itself. There is evidence to support this picture [20]. Indeed, some kind of flow-induced steady state is suggested by the absence of higher-order harmonic responses in our raw waveforms in spite of the fact that the instantaneous velocity varied between zero and v_{peak} during each cycle of oscillation. However, the main point of this experimental study is to describe the dependence on roughness while ignoring the microscopic interpretation.

Deviations from the predictions of the no-slip boundary condition are, alternatively, often represented as the "slip length," the fictive distance inside the solid at which the no-slip flow boundary condition would hold. It is an alternative *empirical* representation of the data just discussed. Mathematical manipulation based on continuum hydrodynamics [21] shows that a given f^* implies a given slip length (b) according to the relation

$$f^* = 2\frac{D}{6b}\left[\left(1 + \frac{D}{6b}\right)\ln\left(1 + \frac{6b}{D}\right) - 1\right]. \qquad (2)$$

Results (Fig. 3, bottom panel) show the implied relations between slip length and flow rate. While it was known previously that a very large amount of roughness is sufficient to generate no slip [10], this appears to present the first quantification of how much actual roughness is needed.

The quantitative dependence on roughness is summarized in Fig. 4. We consider the limits up to which predictions based on the no-slip assumption still described the data (just before they failed). Shear rate, $\dot{\gamma}_{\text{max}}$, was calculated from the relation that, if the stick boundary condition holds in a crossed cylinder geometry, it is proportional to flow rate by a geometrical factor of magnitude between 10^3 and 10^4 that depends on D [21], $\dot{\gamma}_{\text{max}} = A\sqrt{R/D}\, v_{\text{peak}}/D$, where $A = (27/128)^{1/2}$. The shear stress, σ_{peak}, if the stick boundary condition holds, was [21] $\sigma_{\text{peak}} = 3\eta R v_{\text{peak}}/D^2$, where η is the viscosity of bulk liquid. With the shear stress evaluated at the coincident axis of the experiment's curved surfaces, they are plotted against the rms roughness. One observes that they increased rapidly, approximately exponentially, with increasing roughness, with nearly the same dependence for water and tetradecane.

Initially we had expected the wavelength of roughness to matter, but this is not obvious from the data at hand. Though the mean distances between asperities varied

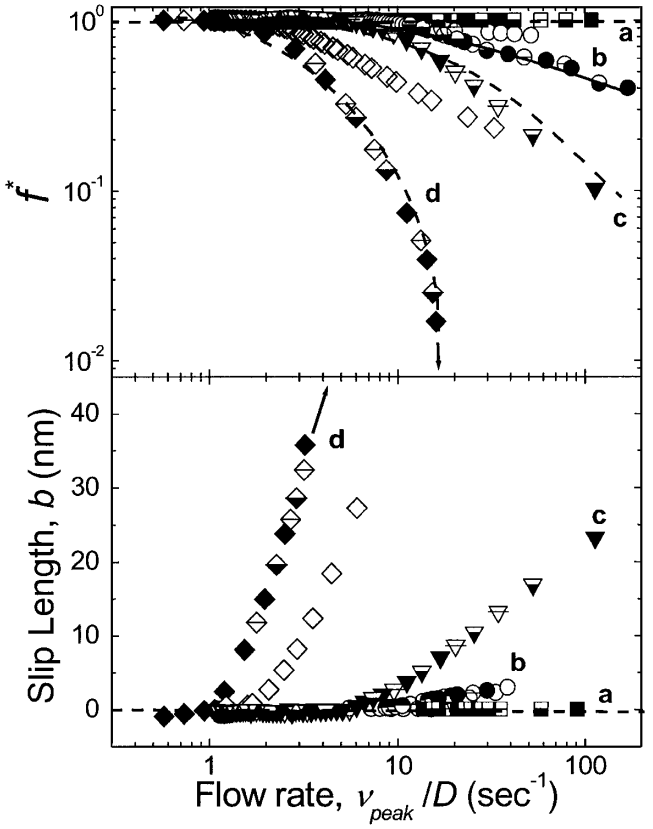

FIG. 3. As a function of logarithmic flow rate, v_{peak}/D, f^* [top panel; f^* is defined in Eq. (1)] and the equivalent slip length (bottom panel) are plotted, for deionized water (filled symbols) and tetradecane (open symbols) flowing between surfaces whose different levels of rms roughness are identified in Table I. Symbols are the same as in Fig. 2. The data, taken at different amplitudes in the range of 0.3–1.5 nm and frequencies in the range 6.3−250 rad sec^{-1}, are mostly not distinguished in order to avoid clutter, since their successful collapse as a function of v_{peak}/D was shown in detail for smooth surfaces previously [12]. To illustrate the similarly successful collapse for these rough surfaces, data taken at the two frequencies 6.3 rad sec^{-1} (cross filled symbols) and 31 rad sec^{-1} (semifilled symbols) for water are included explicitly. In the bottom panel, the slip length (b) was calculated as described in the text.

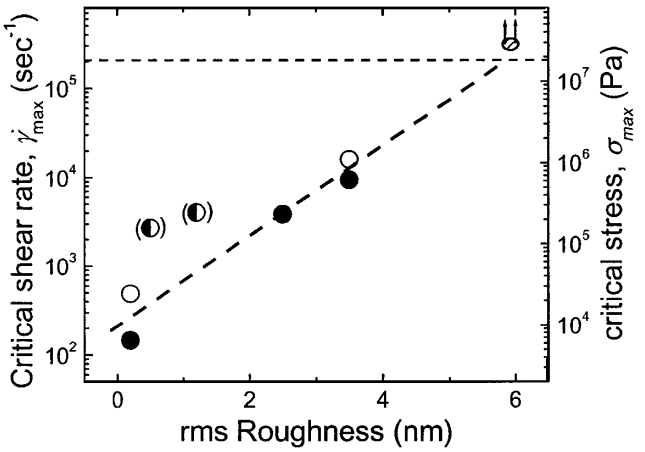

FIG. 4. The critical shear rate for onset of slip (left ordinate) and critical shear stress (right ordinate) are plotted semilogarithmically against rms roughness for flow of deionized water (solid symbols) and tetradecane (open symbols for cases *a*–*c* in Table I and semifilled symbols for cases *e* and *f*). The data in parentheses indicate the asymmetric situation of cases *e* and *f* on one side and case *a* on the other side—one surface was rough and the opposed surface was atomically smooth. Shear rate and shear stress at the coincident apex of the cross cylinders were calculated using known relations based on continuum hydrodynamics [21].

enormously (cf. AFM images in Fig. 1), Fig. 4 reveals remarkably regular dependence on the simpler measure, the root-mean-square roughness. Further work is desirable to extend the available theoretical and simulation analyses [22,23]. The respect in which details of surface texture play a role, and the distinction between topographical and chemical roughness, are at present open issues.

These experiments show, for the first time to the best of our knowledge, how large surface roughness must be to produce the no-slip boundary condition. There are potential implications in applications such as magnetic recording and microfluidics, where roughness can be designed to be very low.

Similarly, there is relevance to the diffusion of molecules in liquid solutions. The transition from "slip" (small, regularly sized molecules) to stick (molecules whose shape is bumpy) has been a concern for a long time [24]. These experiments provide a touchstone for understanding all of these problems.

This work was supported by the National Science Foundation (Tribology Program) with the use of facilities supported by the U.S. Department of Energy, Division of Materials Science through the Frederick Seitz Materials Research Laboratory at the University of Illinois at Urbana-Champaign.

[1] For a historical review, see S. Goldstein, *Modern Developments in Fluid Dynamics* (Clarendon Press, Oxford, 1938), Vol. II, pp. 677–680; see also R. P. Feynman, R. B. Leighton, and M. Sands, *The Feynman Lectures on Physics* (Addison-Wesley, New York, 1963), Vol. II, p. 41-1.
[2] S. Richardson, J. Fluid Mech. **59**, 707 (1973).
[3] K. M. Jansons, Phys. Fluids **31**, 15 (1988).
[4] E. Ruckenstein and P. Rajora, J. Colloid Interface Sci. **96**, 488 (1983).
[5] D. Einzel, P. Panzer, and M. Liu, Phys. Rev. Lett. **64**, 2269 (1990).
[6] P. A. Thompson and M. O. Robbins, Phys. Rev. A **41**, 6830 (1990).
[7] P. A. Thompson and S. Troian, Nature (London) **389**, 360 (1997).
[8] J.-L. Barrat and L. Bocquet, Phys. Rev. Lett. **82**, 4671 (1999).
[9] O. I. Vinogradova, Int. J. Miner. Process. **56**, 31 (1999).
[10] R. Pit, H. Hervet, and L. Léger, Phys. Rev. Lett. **85**, 980 (2000).
[11] V. S. J. Craig, C. Neto, and D. R. M. Williams, Phys. Rev. Lett. **87**, 054504 (2001).
[12] Y. Zhu and S. Granick, Phys. Rev. Lett. **87**, 096105 (2001).
[13] J. S. Peanasky, H. M. Schneider, S. Granick, and C. R. Kessel, Langmuir **11**, 953 (1995).
[14] J. N. Israelachvili, J. Colloid Interface Sci. **110**, 263 (1986).
[15] N. V. Churaev, V. D. Sobolev, and A. N. Somov, J. Colloid Interface Sci. **97**, 574 (1984).
[16] D. Y. C. Chan and R. G. Horn, J. Chem. Phys. **83**, 5311 (1985).
[17] J. M. Georges, S. Millot, J. L. Loubet, and A. Tonck, J. Chem. Phys. **98**, 7345 (1993).
[18] S. Granick, Phys. Today **52**, No. 7, 26 (1999).
[19] P.-G. de Gennes (private communication).
[20] X. Zhang, Y. Zhu, and S. Granick, Science **295**, 663 (2002).
[21] O. I. Vinogradova, Langmuir **11**, 2213 (1995).
[22] A. Jabbarzadeh, J. D. Atkinson, and R. I. Tanner, Phys. Rev. E **61**, 690 (2000).
[23] J. Gao, W. D. Luedtke, and U. Landman, Tribol. Lett. **9**, 3 (2001).
[24] R. Zwanzig, J. Chem. Phys. **68**, 4325 (1978).